

Nanoindentation and contact-mode imaging at high temperatures

Christopher A. Schuh,^{a)} Corinne E. Packard, and Alan C. Lund
*Department of Materials Science and Engineering, Massachusetts Institute of Technology,
Cambridge, Massachusetts 02139*

(Received 8 September 2005; accepted 8 December 2005)

Technical issues surrounding the use of nanoindentation at elevated temperatures are discussed, including heat management, thermal equilibration, instrumental drift, and temperature-induced changes to the shape and properties of the indenter tip. After characterizing and managing these complexities, quantitative mechanical property measurements are performed on a specimen of standard fused silica at temperatures up to 405 °C. The extracted values of hardness and Young's modulus are validated against independent experimental data from conventional mechanical tests, and accuracy comparable to that obtained in standard room-temperature nanoindentation is demonstrated. In situ contact-mode images of the surface at temperature are also presented.

I. INTRODUCTION

With significant recent advances in instrumented nanoindentation testing, it has become possible to routinely measure the mechanical properties of small structures, such as are relevant to microelectronics, microelectromechanical systems, and coatings.^{1–9} For many such applications, it is desirable to measure nanomechanical properties at elevated temperatures (i.e., at relevant service temperatures), but nanoindentation has historically been a room-temperature mechanical testing technique. Although non-instrumented “hot hardness” tests have been used on coarser scales for decades,^{10–15} experimental efforts in high-temperature indentation with load and depth instrumentation have been relatively few. A brief summary of the experimental studies on this topic to date is given in Table I, focusing on the technical conditions of the tests reported. Those studies involving relatively large indentation depths (>1 μm) are denoted as “microscale” studies and differentiated from generally higher-resolution “nano-scale” studies.

Examining Table I, it is clear that the existing studies on elevated-temperature nanoindentation are inhomogeneous, involving different apparatuses, different temperature ranges, and a host of different materials. The properties or physical phenomena under investigation also vary considerably across this literature. For example, Farber et al.^{16,17} have focused on larger

microscale indentations and have studied the energetics of plastic deformation. Lucas and Oliver^{18,19} performed various indentation creep experiments to extract power-law exponents, while Beake, Smith et al.,^{20–22} and Volinsky et al.²³ have looked at the hardness and modulus of various materials at elevated temperature. Recently, a number of authors have studied discrete events under the indenter tip at elevated temperatures, including the displacement burst associated with the elastic-plastic transition in crystals^{24–27} as well as shear band formation in metallic glasses.²⁸ Across all of these various properties and topics, most of the reported studies are concentrated at relatively low temperatures (<200 °C), and closer inspection reveals that higher test temperatures are correlated with lower load and depth resolution, or with generally larger indentations that reduce the relative noise level of the measurement.

Looking at the timeline of the publications in Table I, it is clear that elevated-temperature nanoindentation has been gaining interest in recent years, and we expect that these kinds of measurements will become increasingly important both for fundamental studies of nanomechanical materials properties and for understanding the performance of microdevices. However, the inhomogeneity of the existing literature leaves a number of important issues to be discussed before standard techniques can be established. For example, there has not yet been any unambiguous demonstration that properties such as hardness and modulus can be extracted with precision and accuracy (i.e., in reference to known standards) at high temperatures. Although a number of authors have discussed issues of thermal and electronic drift, there is no

^{a)}Address all correspondence to this author.
e-mail: schuh@mit.edu
DOI: 10.1557/JMR.2006.0080

TABLE I. Summary of fine-scale instrumented indentation studies conducted at elevated temperatures up to T_{\max} . Here micro-scale studies, using indentations typically deeper than 1 μm , are differentiated from nano-scale studies, which use indentation depths generally below one micron. Non-instrumented hot hardness studies are not included in this tabulation.

Year	Authors	Ref.	T_{\max} ($^{\circ}\text{C}$)	Instrument	Material
Micro-scale studies					
1995	Lucas and Oliver	18	75	Similar to MTS Nanoindenter II	In
1998	Farber et al.	16	786	Custom Apparatus	ZrO ₂ -Y ₂ O ₃
1998	Farber et al.	17	396	Custom Apparatus	Ge
1998	Lucas and Oliver	19	75	Similar to MTS Nanoindenter II	In
2001	Fujiwara and Otsuka	45	210	Custom Apparatus	Sn, Pb-Sn
2003	Takagi et al.	46	500	ULVAC-RIKO Custom Apparatus	Al-5.3Mg
2004	Watanabe et al.	47	1137	Custom Apparatus	Thermal barrier oxides
2004	Takagi et al.	48	800	ULVAC-RIKO Custom Apparatus	CMSX-4 Ni alloy
Nano-scale studies					
1996	Suzuki and Ohmura	49	600	Custom Apparatus	Si
1997	Syed-Asif and Pethica	50	50	Custom Apparatus	W, GaAs, In
1999	Bahr et al.	24	106	Custom Apparatus	Fe-3Si
2000	Smith and Zheng	20	200	MicroMaterials NanoTest	Au, Si, soda-lime glass
2001	Wolf et al.	51	120	Hysitron	Y-Mg-Zn
2001	Kramer et al.	25	75	Hysitron Triboscope	W, Fe-3Si
2001	Kraft et al.	52	100	MTS Nanoindenter XP	Al, Al foam
2002	Beake and Smith	21	400	MicroMaterials NanoTest	Au, fused silica, soda-lime glass, polyimide
2003	Beake et al.	22	500	MicroMaterials NanoTest	Various
2003	Xia et al.	53	400	MicroMaterials NanoTest	Fe-40Al
2004	Volinsky et al.	23	130	MTS Nanoindenter II	Au, Pt/Cu
2004	Hinz et al.	54	130	AFM tip, Veeco Dimension 3100	PMMA
2004	Schuh et al.	28	200	Hysitron Triboindenter	Pd- and Mg-based metallic glass
2004	Lund et al.	26	200	Hysitron Triboindenter	Pt
2004	Nieh et al.	55	450	MicroMaterials NanoTest	Zr-based metallic glass
2005	Ma and Komvopoulos	56	78	Hysitron Triboindenter	NiTi
2005	Schuh et al.	27	200	Hysitron Triboindenter	Pt
2005	Zhang et al.	57	200	MicroMaterials NanoTest	NiTi
2006	Present study	...	405	Hysitron Triboindenter	Fused silica

clear consensus as to how severe these issues are, or how they may be characterized and minimized. Additionally, while in situ contact-mode imaging of indentations is now relatively routine at ambient temperature, the limitations of this capability have not been probed in detail at higher temperatures.

The purpose of the present paper is to address the above technical issues with high-temperature nanoindentation experiments ranging up to 405 $^{\circ}\text{C}$, on a specimen of fused silica. Specifically, we quantify drift, equilibration characteristics, and measurement scatter at various temperatures, and outline a procedure that can be used to acquire clean load-displacement data. We also discuss the tip area function at elevated temperatures and the issue of property extraction from load-displacement curves, and demonstrate accurate and precise measurement of hardness and Young's modulus. Finally, we establish the feasibility of in situ contact-mode imaging at temperatures up to 405 $^{\circ}\text{C}$.

II. EXPERIMENTAL SETUP

The experimental apparatus used in this work is based upon the commercial Triboindenter nanoindentation

system from Hysitron, Inc. (Minneapolis, MN). Briefly, the nanoscale control elements of the system include a piezoelectric tube as well as a capacitive transducer; these elements are significantly temperature sensitive. Onto the standard Triboindenter platform, we have added a heating stage and various thermal control elements. The general layout of the system is illustrated in Fig. 1. The system used for thermal management in the present work was based upon a commercial temperature control system manufactured by Hysitron, but extensive customization of many of the components was necessary to achieve the level of performance we report here.

The essential features of the thermal control system include a heating element positioned below the test specimen and a heat shield that thermally isolates the transducer assembly from the heat source. The specimen is mechanically clamped to the copper stage, as the use of adhesives or magnets for specimen mounting is inappropriate at elevated temperatures. The heat source in the present case was a simple resistance element coupled to a power supply. Through use of a J-type thermocouple in contact with the specimen, temperature stability to better than 0.1 $^{\circ}\text{C}$ could be attained at temperatures up to and above 405 $^{\circ}\text{C}$. Although closed-loop control is possible,

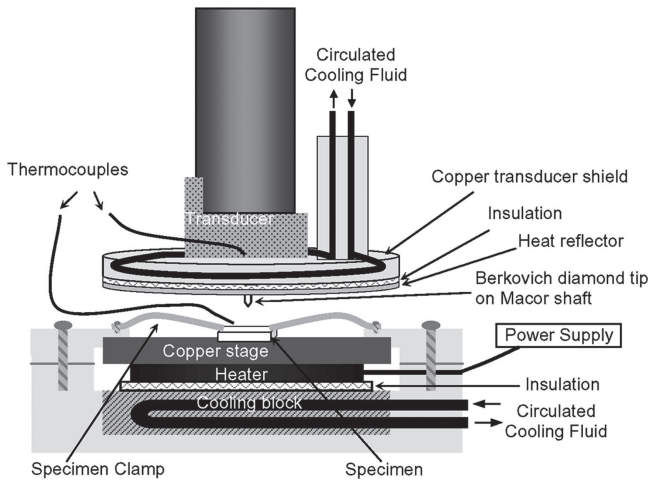


FIG. 1. Schematic illustration of the customized heating stage and peripheral thermal control equipment used in conjunction with the Triboindenter apparatus.

we have found that open-loop temperature control is often more stable if a sufficiently regular heat source and power supply are used.

Due to the extreme thermal sensitivity of the sensing and actuating devices behind the indenter tip, thermal isolation of these components is essential. A cooled copper fixture is used to actively remove heat from the vicinity of these elements, while a low-conductivity insulating layer and a radiative reflector affixed to the bottom of the shield minimize heat transfer from the heated stage below. A second J-type thermocouple located at the transducer is used to monitor the operating temperature of the electronics and to verify that they are not being notably heated. The tip assembly (available from Hysitron, Inc.) consists of a Berkovich geometry diamond tip brazed to a low thermal conductivity Macor shaft. This assembly is attached directly to the transducer element behind the heat shield, and penetrates through a loose hole in the center of the shield.

III. SYSTEM EQUILIBRATION

During a standard room-temperature nanoindentation test there are several potential sources of instrumental drift, including electronic drift from equilibrating sensors and actuators, as well as thermal drift generated by, for example, servo motors that perform coarse positioning operations. In high-temperature nanoindentation, these sources of drift are augmented by additional thermal effects. For example, bringing a cold tip into contact with a heated specimen leads to rapid heat transfer, accompanied by thermal expansion of the tip, transient thermal contraction of the specimen near the contact point, and potentially increased electronic drift if the sensing and actuating devices behind the tip experience higher temperatures. Over longer periods of time, the redistribution

of heat in the environment and load frame may also contribute as a source of drift. Apart from these transient effects, even after contact of the tip with the specimen there are significant potential sources of thermal drift. Slight fluctuations of temperature in the specimen, stage, tip, etc., are all translated into thermal expansions or contractions that superpose upon the true indentation response. For a stage/specimen combination 2 cm tall (as in this work), a thermal fluctuation of ± 1 K can lead to an artificial drift displacement on the order of 100 nm or more; clearly this is enough to severely interfere with a typical nanoindentation experiment with submicron displacement. Furthermore, fluctuation-induced displacements such as these could occur quite gradually, superimposing on the true load–displacement response in a way that is difficult to detect.

The control of instrument drift in high temperature testing requires careful equilibration of the heating system itself, as well as the tip and specimen temperatures. Equilibration of the heating system is relatively straightforward so long as the heat source and cooling systems are stable and constant. The equilibration of the tip with the specimen is generally more complicated. In principle, this may be accomplished through the use of separate heating elements for the specimen and tip,^{20–22} which would each be allowed to equilibrate independently prior to indentation. This approach may be especially appropriate if very deep indentations are desired and the thermal transfer from a heated specimen to unheated tip is insufficient to uniformly warm the tip. In practice, it would be difficult to exactly match the temperatures of the two bodies prior to contact, and some amount of heat redistribution would occur when the tip is brought into contact with the specimen.

In the present work, we have equilibrated the system by bringing the tip, equilibrated first at ambient temperature, into contact with the specimen, equilibrated at the test temperature. As described above, this leads to a significant period of heat redistribution, during which time the drift of the instrument is severe. We have characterized the equilibration characteristics during this period with the following procedure. The first contact of tip with specimen is made with an extremely light set-point load of 1 or 2 μN . From this point on, the tip is not retracted from the specimen surface, but it may be translated across the specimen surface while still in contact. From the time of first contact, indentations are periodically performed, and the drift of the instrument is measured during brief periods of fixed constant load during the indentation. Following standard practice, we begin each indentation with a drift measurement at a very light load (2 μN) and conclude each test with a hold in the 80% unload condition for the same purpose. Between indentations, the tip is relocated to a position remote from those conducted previously (generally a 10 μm spacing

was used in this work), while maintaining contact with the heated specimen for the entire duration of all tests performed at a given temperature.

Following the above procedure, the drift of the system was monitored for the first few hours after the initial contact of the tip with the heated specimen. The results are plotted in Fig. 2, which shows the measured drift rates, with positive values denoting drift of the tip away from the specimen. In this plot results for several different test temperatures are collected and offset from one another along the y axis for clarity; in each case the dashed line denotes zero drift rate. Looking first at the room-temperature data, we see a relatively complex equilibration of the system. In the first few minutes after contact drift occurs in the negative sense, but this quickly evolves to a positive drift rate that remains for a significant amount of time. The system settles into an equilibrated state only after about 40–45 min of sustained tip-specimen contact, beyond which time the drift rate is extremely low and quite stable.

As the test temperature is increased, the details of the equilibration process change as the heat redistribution on contact is more severe and becomes the dominant contribution to drift. At temperatures near 100 °C, the trends in drift rate seen in Fig. 2 remain similar to those measured at room temperature. At higher test temperatures the initial drift rates after contact become much higher, and the amount of time required to reach an equilibrated, steady-state condition increases somewhat. In general,

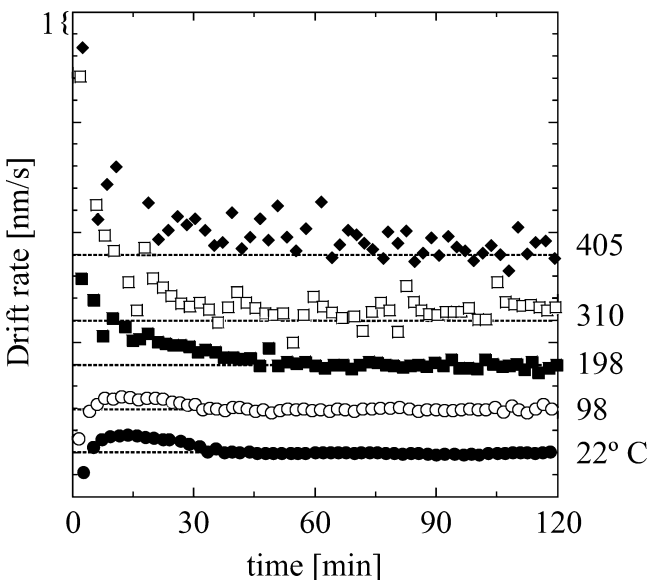


FIG. 2. Equilibration characteristics of the nanoindentation apparatus at various test temperatures; the instantaneous drift rate is plotted as a function of time from the moment of the first tip contact with the hot specimen. The reported values are the average of the pre-indentation and post-indentation (80% unload) measurements. The several data sets are offset along the y axis for clarity of presentation, and the dashed line in each case represents zero drift rate.

60 or 75 min are sufficient to reach the steady state for temperatures up to 405 °C. The level of stability achieved in the steady state also clearly degrades with temperature in Fig. 2 (which will be discussed in Sec. IV), but a steady state condition is achieved in every case. As a final note on this equilibration procedure, we add that in our ongoing work with additional experimental materials, we have found that the same basic equilibration and drift character is seen. These results are more characteristic of the apparatus than they are of the experimental specimen being tested.

IV. STEADY-STATE CONDITION

A. Temperature distribution in steady state

Once the system has been equilibrated at a given test temperature, a question of concern is whether or not the tip, in contact with the heated specimen, is sufficiently uniformly heated over the distance of a typical indentation experiment (several hundred nanometers in the present case). A full analysis of heat transfer, including the complex geometry of the tip assembly and surrounding thermal management devices, as well as conduction and convection of heat in the vicinity of the tip, is beyond our present scope. Instead, we consider a simple one-dimensional heat transfer model to approximately assess the uniformity of heating in the diamond tip. Since the tip of the diamond is in direct mechanical contact with the specimen, and the surface temperature of the specimen is known, it is reasonable to assume that the very tip of the diamond experiences the applied test temperature in steady state. Behind the contact point, the tip is heated by conduction of heat backwards from the contact, and likely also by significant convective transport from the specimen. Neglecting the contribution of convection, the conduction case provides a lower-bound on the amount of heat introduced into the diamond tip. If heat is lost primarily through conduction along the load column, then the situation becomes a simple problem of temperature gradient partitioning between the diamond tip and the Macor shaft to which it is mounted. The steady-state solution of the conduction equation in one dimension gives²⁹

$$\frac{\Delta T_d}{\Delta T_M} = \frac{t_d}{t_M} \cdot \frac{D_M}{D_d} \quad (1)$$

Here ΔT represents the temperature drop over the thickness t , given thermal diffusivities D ; the subscripts denote properties in the diamond tip (d) and Macor shaft (M). For the indenter tip assembly used in this work, the diamond tip is very small compared to the load column, $t_d/t_M \approx 40 \mu\text{m}/8 \text{ mm} \approx 5 \times 10^{-3}$, and the disparity between the thermal diffusivities is also quite large,^{30,31} $D_M/D_d \approx 7 \times 10^{-7} \text{ m}^2 \text{ s}^{-1}/10^{-3} \text{ m}^2 \text{ s}^{-1} \approx 7 \times 10^{-4}$.

Accordingly the temperature gradient through the diamond is extremely small according to Eq. (1), ΔT_d being considerably less than one degree for any of the test temperatures used in this work. Due to the low thermal conductivity of the Macor load column, heat is sequestered in the diamond tip, which is evenly heated to an appreciable distance away from the contact point. It is worth noting that additional elements added in series (e.g., the braze material used to attach the diamond to the Macor) do not affect the validity of Eq. (1) or the general scaling relations captured there. Based on this simple calculation, we believe that the tip heating in the present configuration is likely sufficient, provided that the instrument is adequately equilibrated.

B. Instrumental drift in steady state

An important point revealed by Fig. 2 is that even once the equilibrated state has been reached, the instantaneous drift rate of the instrument can be quite high. The scatter in the steady-state drift rate clearly increases as the test temperature rises, and at the highest temperatures studied here is quite appreciable, sometimes exceeding ± 1 nm/s. We believe this drift is associated with minor thermal fluctuations and the associated expansions and contractions, or perhaps with convective airflow around the indenter tip. In any event, this steady-state drift is an important issue for reliable extraction of mechanical properties, and with our present apparatus it is an inevitable consequence of testing at high temperatures.

Since thermal drift apparently cannot be entirely eliminated in our present system, it must be understood and managed as best as possible. We propose the following general procedure to characterize the steady-state drift properties of a given apparatus. We begin by thermally equilibrating the apparatus in the manner described above, with the tip held in contact with the specimen for about 75 min. After equilibration, a series of identical indentations is made for the sole purpose of analyzing the statistics of drift, using the standard 80% unload drift measurement. As before, the indenter must be relocated between indentations, while maintaining contact with the heated specimen below. Enough indentations must be performed to produce a reliable statistical data set; we have generally used 50 or more at each test temperature.

The statistical data acquired in the manner outlined above can be assembled into a “master drift plot,” which plots drift rate as a function of the test temperature, and represents the statistics using contours of cumulative probability. An example of a master drift plot is shown in Fig. 3, and by reading the contours at a given test temperature, one can quickly identify the probability that a given indentation will have a drift rate equal to or below the indicated value. For example, at room temperature, the data show that 100% of the tests had a drift rate at or below ~ 0.12 nm/s. As the temperature is increased, the

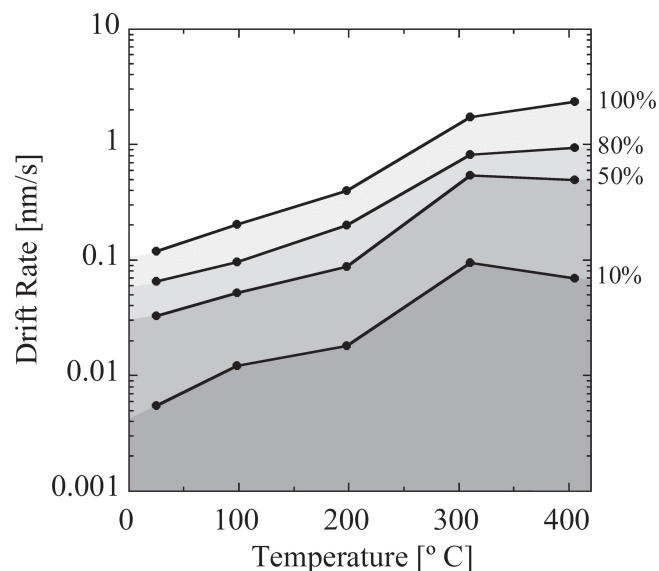


FIG. 3. Master drift plot characterizing the steady-state behavior of the present nanoindentation apparatus. The contour lines represent the fraction of tests with drift rate equal to or below the plotted value.

contours all tend toward higher drift rates; at 405 °C, we see that 100% of the tests exhibited drift rates below about 2.4 nm/s, but only a small fraction of tests ($\sim 10\%$) had a drift rate below 0.1 nm/s.

From a practical point of view, Fig. 3 can be used to estimate the expected yield of acceptable data from a series of indentations under a given set of conditions. Based upon the material being studied and the typical depth and time of an indentation, an “acceptable” drift rate can be identified. For example, for our study of fused silica, we perform indentations of typical depth ~ 300 nm, and we require that the error on this depth be no more than $\pm 1\%$ (± 3 nm) over a typical duration of ~ 10 s. This requires a drift rate below about 0.3 nm/s. Referring to Fig. 3, we see that this poses no particular problem for test temperatures below about 200 °C, for which virtually every experiment can be expected to have drift rates in the acceptable range. At higher temperatures, some fraction of the indentations performed will “fail” on the basis of drift, and only a fraction of the indentations performed will have acceptable drift rates. Clearly, time is a critical parameter in these calculations; longer indentations are prone to increased drift error, so researchers intending to perform long indentations must be especially careful to understand and control drift. Alternatively, relatively quicker indentations can be used to avoid significant drift displacements, although cognizance of rate-sensitivity in the experimental material is required to intelligently use this approach. Nonetheless, for indentations on fused silica 10 s in duration the yield of acceptable data is ~ 0.5 even at the highest temperatures used here, so it remains possible, in principle, to measure mechanical properties up to 405 °C.

It must be emphasized that the master drift plot in Fig. 3 is a characteristic of the particular experimental setup used in the present work, and represents a starting point for improving the drift properties of high-temperature nanoindentation systems. We expect that refinements to the heating and thermal management hardware used in these tests could change the shape of the contours in Fig. 3, ideally lowering them uniformly and reducing their slopes significantly. Furthermore, master drift plots could be constructed for different nanoindentation apparatuses, and used as a means of comparison; the effects of, e.g., horizontal tip orientation or tip heating elements could thereby be assessed directly.

V. HARDNESS AND MODULUS MEASUREMENT

A. Tip area function

The accurate extraction of mechanical properties by nanoindentation relies upon a reasonable mathematical description of the tip geometry, usually through quantitative calibration of the empirical tip area function. This function relates the projected contact area A_p to the contact depth of the indentation h_c and may be expressed as, e.g., a polynomial function or an interpolation table. Although calibration procedures for the area function are now well established at ambient temperatures, there has been no quantitative discussion surrounding the use of the area function at elevated temperatures. Before attempting to measure hardness and modulus at elevated temperatures, we examine the expected effects of temperature upon the area function.

For purposes of mathematical simplicity, we will use in our discussion the analytical form for A_p proposed by Thurn and Cook³²:

$$A_p = \frac{\pi}{\cot^2 \theta} \cdot h_c^2 + 4\pi \cdot R \cdot h_c + 4\pi \cdot R^2 \cdot \cot^2 \theta \quad (2)$$

This area function was constructed on a geometric basis by imagining the tip shape as a superposition of two geometries: a sharp self-similar shape described by its included half-angle θ and a sphere described by its radius R . This function succinctly captures the general form of “sharp” indenters used in nanoindentation, which are designed in self-similar geometries like the Berkovich pyramid (for which $\theta = 70.8^\circ$) but which exhibit inevitable rounding at the tip. Thurn and Cook have shown that this function can be reasonably used in lieu of the more common Oliver–Pharr polynomial function (which was constructed only as an empirical means of describing A_p ^{2,33}).

The form of Eq. (2) is particularly useful for estimating the effect of temperature on the tip area function because the two superposed geometries can be treated essentially independently. Our main concern here is that

the parameters that describe the tip (R and θ) may change upon heating. For an indenter tip composed of a cubic material (e.g., diamond), the thermal expansion will be isotropic, and the self-similar macroscopic geometry of the tip will be preserved; θ is safely taken as independent of temperature. On the other hand, the rounded portion of the tip is not self-similar and will expand proportionally with temperature as

$$\frac{dR}{dT} = \alpha \cdot R \quad (3)$$

where α is introduced as the coefficient of thermal expansion ($\approx 5 \times 10^{-7} \text{ K}^{-1}$ for diamond³⁴). The total effect of temperature on the tip area function is then written as

$$\frac{dA_p}{dT} = 4\pi \cdot \alpha \cdot R \cdot [h_c + 2 \cdot R \cdot \cot^2 \theta] \quad (4)$$

If the area function is calibrated at room temperature T_o , the thermal excursion can be taken as $dT \approx (T - T_o)$. For a tip of known geometry, Eq. (4) is easily evaluated to assess the effect of temperature on A_p , as shown in Fig. 4. Here we plot the percentage change of A_p with respect to its calibrated value at room temperature, as a function of indentation depth and for various typical values of the blunting radius R . To assess the worst-case scenario for our experiments, we have taken a thermal excursion of $dT = 400 \text{ K}$; the results for lower test temperatures would be proportionally reduced.

Several trends emerge from Fig. 4. First, we see that sharper tips in general are less susceptible to thermally-induced error in A_p , a natural result given that the self-similar portion of the indenter behind the tip is geometrically invariant with temperature changes. Second, and

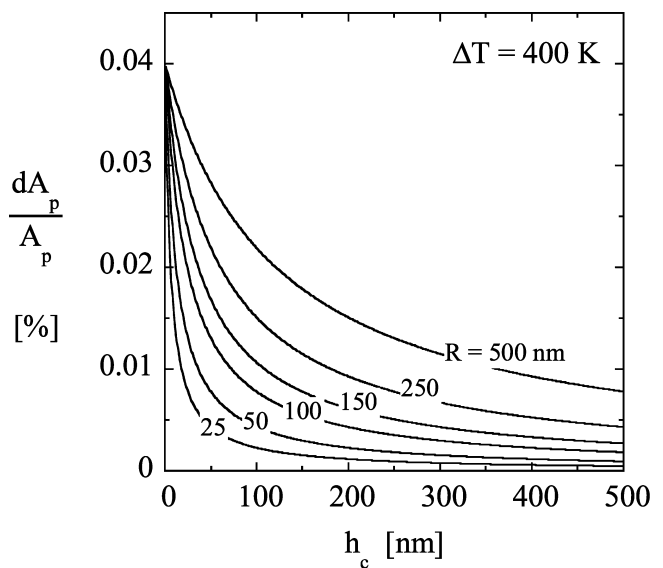


FIG. 4. Relative change in the tip area function as a function of contact depth, after a thermal excursion of 400 K. Calculations are based on Eq. (4) for assumed values of the tip radius R .

more importantly, the errors on A_p decay rapidly with indentation depth and are generally quite negligible at the typical depths used for property measurement ($h_c > R$). In fact, the error calculated at virtually any depth is quite negligible, being in the worst case about 0.04% for extremely shallow indentations (with any tip radius). This error is certainly on or below the scale of uncertainty in the calibration of A_p in the first place, so we can reasonably conclude that the effect of temperature on the area function is generally negligible. We have verified this expectation by performing a standard area function calibration at several temperatures up to 405 °C, using the temperature-dependent Young's modulus of fused silica (discussed in more detail below); no change in the area function could be discerned, and the load-frame compliance was also found to be insensitive to test temperature. For the purposes of property measurement, we conclude that it is reasonable to calibrate the area function using standard practices at room temperature, and then take the same function to be valid at elevated test temperatures; this is the procedure we have followed here.

B. Measured properties

Using the best procedures developed above, we have evaluated the hardness H and reduced indentation modulus E_R of fused silica at eight different test temperatures between room temperature and 405 °C, using loading rates between 2 and 10 mN/s. The glass used for this purpose was grade "N" high-purity fused silica manufactured by Tosoh SGM USA (Flemington, NJ), prepared through a standard regimen of mechanical polishing to better than 2 nm rms roughness. This material is provided as a standard for calibration of the nanoindenter, due to its highly consistent and depth-independent properties.^{35–37} Some typical load–displacement (P - h) curves are shown in Fig. 5, reflecting the effect of temperature on the measured response. The drift statistics obtained from these measurements were in line with the master drift plot of Fig. 3, and only tests with total drift errors below 3 nm were accepted for property evaluation. The generally low drift rates obtained are reflected in the minor perturbations at the 80% unload condition in the curves of Fig. 5, where a 10-s hold was performed.

The hardnesses and reduced moduli obtained from these experiments are plotted as a function of the test temperature in Figs. 6(a) and 6(b), respectively. The reported values represent an average of at least 20 separate measurements, each of which was evaluated using the standard Oliver–Pharr method based on the unloading portion of the P - h curve. The error bars on the data in Fig. 6 represent the standard deviation of the tests; although the scatter in the measurements increases with temperature, the trends we have measured are clearly larger than the measurement error. In fact, the standard deviation of these tests was within about 5% of the mean

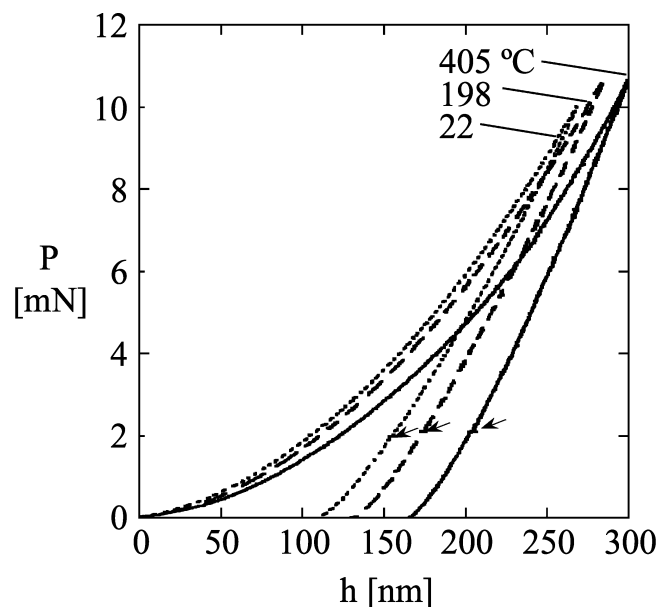


FIG. 5. Typical load–displacement (P - h) curves obtained in the present study at temperatures over the full tested range (22–405 °C) and 2 mN/s loading rate. The arrows denote the location of the hold period at 80% unload.

value at all of the test temperatures, which is within the typical accuracy of nanoindentation property measurements at room temperature. We conclude from this result that drift and measurement scatter should not pose a fundamental barrier to accurate property measurements using high temperature nanoindentation.

C. Accuracy of measured properties

To our knowledge, there is only one prior study that used nanoindentation to extract the hardness and reduced modulus of fused silica at elevated temperatures. The work of Beake et al.^{21,22} used a very different apparatus from ours (compare with Table I), and obtained somewhat different results, as can be seen in Fig. 6. Both sets of data show an increase in modulus and a decrease in hardness with increasing test temperature, but the severity of these trends is significantly different in the two studies. Since there has not previously been any validation of high-temperature nanoindentation for quantitative property measurements, it is not immediately clear which set of measurements (if any) represents an accurate picture of the temperature-dependent properties of silica. To address this issue, we now turn our attention to judging the accuracy of these values through comparison with independent data measured using more conventional methods.

In the case of hardness, the appropriate comparison for our nanoindentation experiments would be conventional microhardness measurements based on optical measurements of the indentation area. The Handbook of Glass

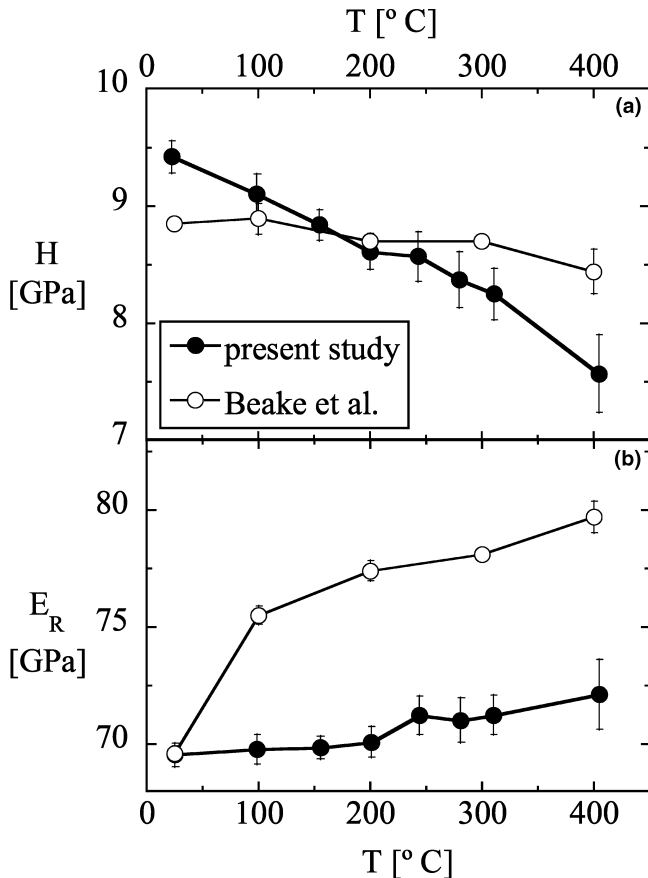


FIG. 6. Measured values of (a) hardness and (b) reduced indentation modulus from our nanoindentation experiments on fused silica with a loading rate of 10 mN/s. Plotted values represent an average of 20 or more indentations, and the error bars represent the standard deviation of the measurement. Plotted for comparison are the data of Beake et al.,^{21,22} also acquired by nanoindentation of fused silica, but using a different apparatus.

Data³⁸ gives three relevant sets of hot hardness data for silica glass of nominally high purity. These data are variable from one glass to the next, but do all soften with temperature over our range of experimental temperatures. The slopes of these softening trends range from $dH/dT \approx -2.8$ to -6.9 MPa/K, with an average slope of -4.4 MPa/K. In comparison, our data follow a roughly linear softening trend with a slope $dH/dT \approx -4.5$ MPa/K, which is in remarkable agreement with the literature values given above, especially since the mechanisms of deformation may be different at our low nanoindentation loads, as compared with much larger microindentation loads; the former experiments exhibit no cracking and are dominated by plastic flow and densification, while the latter are commonly dominated by cracking. The data of Beake et al.^{21,22} [Fig. 6(b)] give a lower hardness slope of $dH/dT \approx -1.0$ MPa/K over the same range of experimental temperatures, and this value is also of the correct order.

In the case of elevated temperature elastic properties, there is an abundance of experimental literature that reports measurements on fused silica, obtained predominantly using acoustic techniques.^{39–42} The reduced modulus measured in our nanoindentation experiments is a composite elastic parameter that includes properties of both silica and the diamond indenter tip, according to¹

$$\frac{1}{E_R} = \left(\frac{1 - \nu_d^2}{E_d} \right) + \left(\frac{1 - \nu_s^2}{E_s} \right), \quad (5)$$

where E is Young's modulus and ν is Poisson's ratio, and the subscripts d and s refer to the properties of diamond and silica, respectively. Equation (5) can be used to extract the Young's modulus of silica from the measured values of E_R , provided that ν is known for the specimen, and both E and ν are known for the diamond tip. Poisson's ratio is usually well-approximated as temperature independent, so the standard values $\nu = 0.17$ and 0.07 can be used for silica and diamond, respectively. However, the Young's modulus of diamond decreases with temperature, and this must be accounted for in Eq. (5). Here we use an empirical expression given by Szuets et al.⁴³ based on a fit to experimental data from a number of different studies:

$$E_d = E_d^{RT} \cdot [1 + c \cdot (T - 293)] \quad (6)$$

where the superscript RT denotes the room temperature modulus, and $c = -1.027 \times 10^{-4} \text{ K}^{-1}$ is an empirical constant. In the present case, the diamond tip is much

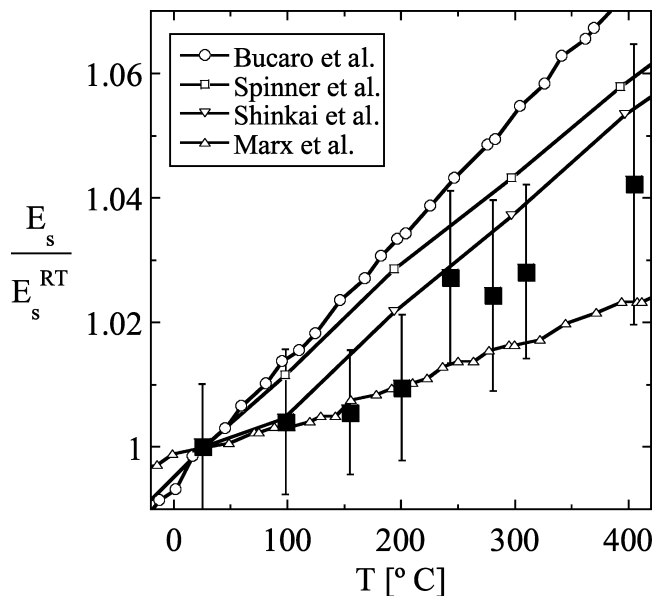


FIG. 7. Extracted values of the Young's modulus of fused silica, based on the data in Fig. 6 and Eqs. (5) and (6). The data are normalized by the modulus at room temperature (E_s^{RT}) to better compare with the literature data of Bucaro et al.,⁴² Spinner et al.,⁴¹ Shinkai et al.,³⁹ and Marx et al.⁴⁰

stiffer than the silica substrate, and the small change ($\sim 4\%$) in diamond's modulus at temperatures up to $405\text{ }^\circ\text{C}$ has only a minor effect on the extracted Young's modulus of silica. Nonetheless, Eq. (6) is included here for completeness, and we note that this effect may be more significant for other experimental materials or for tests performed at higher temperatures [although it should be noted that Eq. (6) breaks down where diamond becomes unstable to the formation of graphite; this can be as low as $500\text{ }^\circ\text{C}$ depending on the local environment⁴⁴].

Figure 7 plots the extracted values for the Young's modulus of silica, normalized by the value obtained at room temperature, $E_s^{\text{RT}} = 71.9\text{ GPa}$. As the test temperature increases, the modulus increases slightly, by about 1% for every 100 K. The trend of the experimental data is linear to within the error of the measurement, and as seen in Fig. 7, is very much in line with prior measurements made by different methods. It should be noted that the acoustic measurements shown in Fig. 7 are performed without a significant hydrostatic overpressure, while the

present indentation measurements inherently produce a significant hydrostatic stress field in the measured volume. In spite of this difference, the magnitudes of the measurements are in good agreement.

The only prior nanoindentation measurements of the high-temperature elastic response of silica are those of Beake et al. [Fig. 6(b)]. Those authors did report the correct sign of the modulus temperature coefficient (i.e., they observed increased stiffness at higher temperatures), but with a higher slope than we see here. Although their data [Fig. 6(b)] have not been replotted in Fig. 7, their extracted values are considerably higher than all of the data shown there (reaching E_s/E_s^{RT} values above 1.10). There are many possible explanations for this disagreement; we note that the experiments of Beake et al. used much higher peak loads ($\sim 200\text{ mN}$ compared with 10 mN here), and given comparable indentation loading rates to ours, this would lead to much longer indentation times. These differences have implications both for the potential deformation mechanisms accessed (e.g., different degrees of densification, possible devitrification or

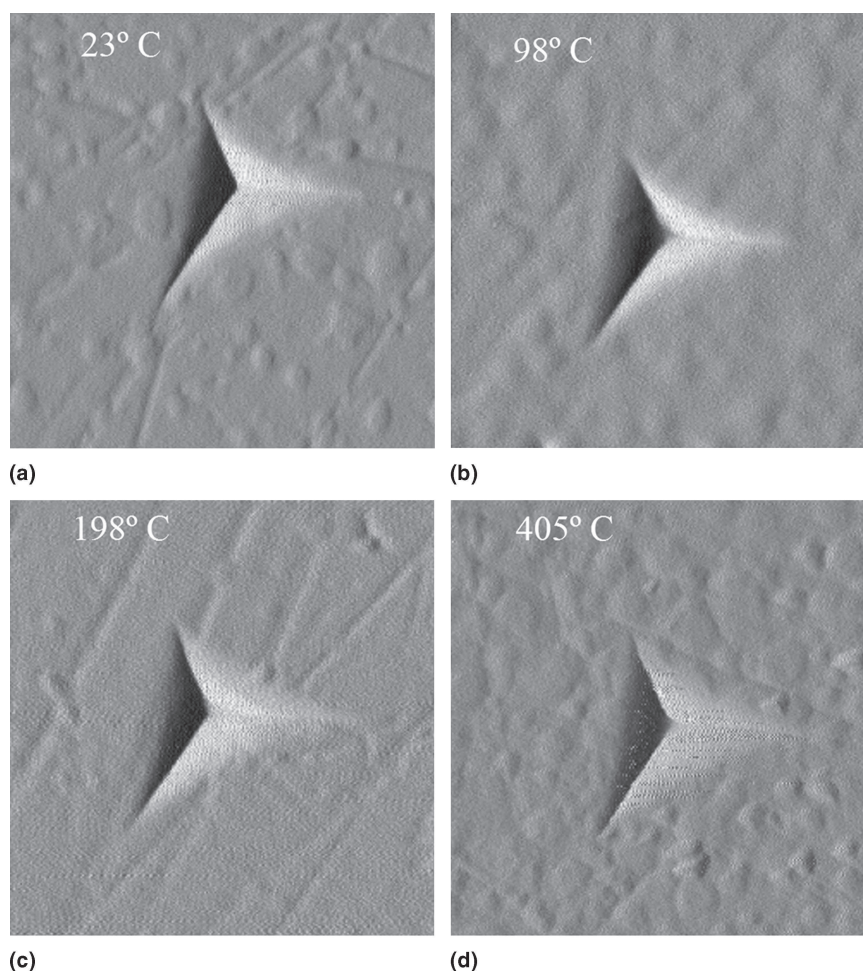


FIG. 8. Gradient images of Berkovich indentations performed at (a) $23\text{ }^\circ\text{C}$, (b) $98\text{ }^\circ\text{C}$, (c) $198\text{ }^\circ\text{C}$, and (d) $405\text{ }^\circ\text{C}$, and imaged in situ with the indenter tip in contact mode at the test temperature. Each image is $3.5\text{ }\mu\text{m}$ in width.

cracking at high loads), and the required stability of the apparatus.

To summarize the above discussion, we have extracted the hardness and Young's modulus of standard fused silica over the temperature range from 23 to 405 °C, and both of these parameters are in quantitative agreement with prior experimental literature. To our knowledge, this is the first time that high-temperature nanoindentation data have been successfully validated against independent mechanical test data, which opens the door for quantitative application of the technique for measurement of unknown materials properties. Additionally, in the specific case of fused silica, accurate high-temperature nanoindentation experiments will allow for fundamental studies of the physics and mechanisms of deformation as a function of temperature (e.g., densification versus shear flow processes, effects of mechanically or thermally induced devitrification, etc.). Provided that these physics are reproducible and robust, we see no fundamental barrier to the use of fused silica as a high-temperature calibration standard for nanoindentation, at least at temperatures below the softening point.

VI. CONTACT MODE IMAGING

The present nanoindentation technique requires a sustained contact between the specimen and the indenter tip, and for most of this contact period the applied load is extremely low ($\sim 2 \mu\text{N}$). In this condition, it is possible to use the indenter tip for contact-mode imaging by recording displacements at constant load as the tip is rastered over the specimen surface. This technique is common at room temperature (especially with the Hysitron Triboindenter apparatus), and here we extend the technique to 405 °C. Figure 8 shows four contact-mode images (gradient view) of indentations in fused silica, performed with a maximum applied load of 10 mN at each of four different test temperatures. The images themselves were acquired in situ at the respective test temperatures and show indentations that look essentially similar to one another. This observation is in line with the similar P - h responses recorded at these test temperatures (Fig. 5), and with expectations based on the mechanics of silica glass in the temperature range of interest. The images in Fig. 8 demonstrate the use of contact-mode imaging at elevated temperature, and it is hoped that in future studies this capability might help shed insight into, e.g., the effect of temperature on pileup around the indenter.

VII. CONCLUSIONS

We have presented a technique for high-temperature nanoindentation studies as well as contact-mode imaging at temperatures up to 405 °C. A number of technical

issues have been addressed to successfully apply the technique:

(1) Provided that the diamond indenter tip is affixed to a low thermal conductivity shaft, it is possible to heat the tip through its contact with a hot specimen. The redistribution of heat after contact can take up to 75 min, which is identified as the characteristic equilibration time of the present apparatus. Indentations must be performed while maintaining constant contact between tip and surface; the tip is relocated from one position to the next at a very low imaging load.

(2) After thermal equilibration at an elevated test temperature, there can be significant instrumental drift in the steady state condition. The steady-state drift character of an apparatus can be represented statistically in a "master drift plot," which can be used to guide the selection of test loads and durations.

(3) Quantitative extraction of hardness and modulus at high temperatures is possible using the standard Oliver-Pharr method, since the effect of thermal expansion on the tip area function is essentially negligible. The change of elastic modulus of diamond with temperature is also relatively small and can be corrected for.

Using the best practices learned from these analyses, we have demonstrated the possibility of in situ contact-mode imaging at temperature and have measured the hardness and Young's modulus of fused silica as a function of temperature from 23 to 405 °C. Unlike prior high-temperature nanoindentation efforts, we have demonstrated quantitative agreement with literature data for these properties, validating the use of nanoindentation for elevated-temperature property measurement.

ACKNOWLEDGMENTS

This work was supported by the Office of Naval Research, Grant No. N00014-04-1-0669; the views expressed herein are not endorsed by the sponsor. Collaborative support of Hysitron, Inc., is gratefully recognized, and C.E.P. acknowledges support of the Ida M. Green Fellowship at MIT.

REFERENCES

1. B. Bhushan: Nanomechanical properties of solid surfaces and thin films, in *Handbook of Micro/Nano Tribology*, edited by B. Bhushan (CRC Press, Boca Raton, FL, 1999), p. 433.
2. W.C. Oliver and G.M. Pharr: An improved technique for determining hardness and elastic modulus using load and displacement sensing indentation experiments. *J. Mater. Res.* **7**, 1564 (1992).
3. T.A. Venkatesh, K.J. Van Vliet, A.E. Giannakopoulos, and S. Suresh: Determination of elasto-plastic properties by instrumented sharp indentation: Guidelines for property extraction. *Scripta Mater.* **42**, 833 (2000).

4. R. Saha and W.D. Nix: Effects of the substrate on the determination of thin film mechanical properties by nanoindentation. *Acta Mater.* **50**, 23 (2002).
5. A.C. Fischer-Cripps: *Nanoindentation* (Springer, New York, 2002).
6. G. Feng and A.H.W. Ngan: Effects of creep and thermal drift on modulus measurement using depth-sensing indentation. *J. Mater. Res.* **17**, 660 (2002).
7. S. Suresh, T.G. Nieh, and B.W. Choi: Nano-indentation of copper thin films on silicon substrates. *Scripta Mater.* **41**, 951 (1999).
8. N.I. Tymiak, D.E. Kramer, D.F. Bahr, J.T. Wyrobek, and W.W. Gerberich: Plastic strain and strain gradients at very small indentation depths. *Acta Mater.* **49**, 1021 (2001).
9. Y. Choi and S. Suresh: Nanoindentation of patterned metal lines on a Si substrate. *Scripta Mater.* **48**, 249 (2003).
10. A.G. Atkins, A. Silverio, and D. Tabor: Indentation hardness and the creep of solids. *J. Inst. Met.* **94**, 369 (1966).
11. T.O. Mulhearn and D. Tabor: Creep and hardness of metals: A physical study. *J. Inst. Met.* **89**, 7 (1960).
12. T.R.G. Kutty, C. Ganguly, and D.H. Sastry: Development of creep curves from hot indentation hardness data. *Scripta Mater.* **34**, 1833 (1996).
13. W.B. Li, J.L. Henshall, R.M. Hooper, and K.E. Easterling: The mechanisms of indentation creep. *Acta Metall. Mater.* **39**, 3099 (1991).
14. P.M. Sargent and M.F. Ashby: Indentation creep. *Mater. Sci. Technol.* **8**, 594 (1992).
15. B.Y. Farber, S.Y. Yoon, K.P.D. Lagerlof, and A.H. Heuer: Microplasticity during high-temperature indentation and the Peierls potential in sapphire (α -Al₂O₃) single-crystals. *Phys. Status Solidi A* **137**, 485 (1993).
16. B.Y. Farber, V.I. Orlov, and A.H. Heuer: Energy dissipation during high-temperature displacement-sensitive indentation in cubic zirconia single crystals. *Phys. Status Solidi A* **166**, 115 (1998).
17. B.Y. Farber, V.I. Orlov, V.I. Nykitenko, and A.H. Heuer: Mechanisms of energy dissipation during displacement-sensitive indentation in Ge single crystals at elevated temperatures. *Philos. Mag.* **A78**, 671 (1998).
18. B.N. Lucas and W.C. Oliver: Time dependent indentation testing at non-ambient temperatures utilizing the high temperature mechanical properties microprobe, in *Thin Films: Stresses and Mechanical Properties V*, edited by S.P. Baker, C.A. Ross, P.H. Townsend, C.A. Volkert, and P. Børgesen (Mater. Res. Soc. Symp. Proc. **356**, Pittsburgh, PA, 1995), p. 137.
19. B.N. Lucas and W.C. Oliver: Indentation power-law creep of high-purity indium. *Metall. Mater. Trans.* **30A**, 601 (1999).
20. J.F. Smith and S. Zheng: High temperature nanoscale mechanical property measurements. *Surf. Eng.* **16**, 143 (2000).
21. B.D. Beake and J.F. Smith: High-temperature nanoindentation testing of fused silica and other materials. *Philos. Mag.* **A82**, 2179 (2002).
22. B.D. Beake, S.R. Goodes, and J.F. Smith: Nanoscale materials testing under industrially relevant conditions: High-temperature nanoindentation testing. *Z. Metallkde.* **94**, 798 (2003).
23. A.A. Volinsky, N.R. Moody, and W.W. Gerberich: Nanoindentation of Au and Pt/Cu thin films at elevated temperatures. *J. Mater. Res.* **19**, 2650 (2004).
24. D.F. Bahr, D.E. Wilson, and D.A. Crowson: Energy considerations regarding yield points during indentation. *J. Mater. Res.* **14**, 2269 (1999).
25. D.E. Kramer, K.B. Yoder, and W.W. Gerberich: Surface constrained plasticity: Oxide rupture and the yield point process. *Philos. Mag.* **A81**, 2033 (2001).
26. A.C. Lund, A.M. Hodge, and C.A. Schuh: Incipient plasticity during nanoindentation at elevated temperatures. *Appl. Phys. Lett.* **85**, 1362 (2004).
27. C.A. Schuh, J.K. Mason, and A.C. Lund: Quantitative insight into dislocation nucleation from high temperature nanoindentation experiments. *Nat. Mater.* **4**, 617 (2005).
28. C.A. Schuh, A.C. Lund, and T.G. Nieh: New regime of homogeneous flow in the deformation map of metallic glasses: Elevated temperature nanoindentation experiments and mechanistic modeling. *Acta Mater.* **52**, 5879 (2004).
29. H.S. Carslaw and J.C. Jaeger: *Conduction of Heat in Solids* (Clarendon Press, Oxford, UK, 1959).
30. J.E. Graebner, S. Jin, G.W. Kammlott, J.A. Herb, and C.F. Gardinier: Large anisotropic thermal-conductivity in synthetic diamond films. *Nature* **359**, 401 (1992).
31. Technical data sheet, Macor, Corning, Inc., Corning, NY.
32. J. Thurn and R.F. Cook: Simplified area function for sharp indenter tips in depth-sensing indentation. *J. Mater. Res.* **17**, 1143 (2002).
33. W.C. Oliver and G.M. Pharr: Measurement of hardness and elastic modulus by instrumented indentation: Advances in understanding and refinements to methodology. *J. Mater. Res.* **19**, 3 (2004).
34. T.W. Clyne and P.J. Withers: *An Introduction to Metal Matrix Composites* (Cambridge University Press, Cambridge, UK, 1993).
35. A.J. Bushby and D.J. Dunstan: Plasticity size effects in nanoindentation. *J. Mater. Res.* **19**, 137 (2004).
36. M. Sukanuma and M.V. Swain: Simple method and critical comparison of frame compliance and indenter area function for nanoindentation. *J. Mater. Res.* **19**, 3490 (2004).
37. K. Herrmann, N.M. Jennett, S. Kuypers, I. McEntegart, C. Ingelbrecht, U. Hangen, T. Chudoba, F. Pohlenz, and F. Menelao: Investigation of the properties of candidate reference materials suited for the calibration of nanoindentation instruments. *Z. Metallkde.* **94**, 802 (2003).
38. *Handbook of Glass Data*, edited by O.V. Mazurin, M.V. Streltsina, and T.P. Shvaiko-Shvaikovskaya (Elsevier, Amsterdam, The Netherlands, 1983).
39. N. Shinkai, R.C. Bradt, and G.E. Rindone: Fracture-toughness of fused SiO₂ and float glass at elevated-temperatures. *J. Am. Ceram. Soc.* **64**, 426 (1981).
40. J.W. Marx and J.M. Sivertsen: Temperature dependence of the elastic moduli and internal friction of silica and glass. *J. Appl. Phys.* **24**, 81 (1953).
41. S. Spinner and G.W. Cleek: Temperature dependence of Young's modulus of vitreous germania and silica. *J. Appl. Phys.* **31**, 1407 (1960).
42. J.A. Bucaro and H.D. Dardy: High-temperature Brillouin scattering in fused quartz. *J. Appl. Phys.* **45**, 5324 (1974).
43. F. Szeucs, M. Werner, R.S. Sussmann, C.S.J. Pickles, and H.J. Fecht: Temperature dependence of Young's modulus and degradation of chemical vapor deposited diamond. *J. Appl. Phys.* **86**, 6010 (1999).
44. H.O. Pierson: *Handbook of Carbon, Graphite, Diamond, and Fullerenes* (Noyes Publications, Park Ridge, NJ, 1993).
45. M. Fujiwara and M. Otsuka: Indentation creep of beta-Sn and Sn-Pb eutectic alloy. *Mater. Sci. Eng.* **319**, 929 (2001).
46. H. Takagi, M. Dao, M. Fujiwara, and M. Otsuka: Experimental and computational creep characterization of Al-Mg solid-solution alloy through instrumented indentation. *Philos. Mag.* **83**, 3959 (2003).
47. M. Watanabe, C. Mercer, C.G. Levi, and A.G. Evans: A probe for the high temperature deformation of thermal barrier oxides. *Acta Mater.* **52**, 1479 (2004).
48. H. Takagi, M. Fujiwara, and K. Takehi: Measuring Young's

- modulus of Ni-based superalloy single crystals at elevated temperatures through microindentation. *Mater. Sci. Eng.* **A387–89**, 348 (2004).
49. T. Suzuki and T. Ohmura: Ultra-microindentation of silicon at elevated temperatures. *Philos. Mag.* **A74**, 1073 (1996).
 50. S.A. Syed-Asif and J.B. Pethica: Nanoindentation creep of single-crystal tungsten and gallium arsenide. *Philos. Mag.* **A76**, 1105 (1997).
 51. B. Wolf, K.O. Bambauer, and P. Paufler: On the temperature dependence of the hardness of quasicrystals. *Mater. Sci. Eng.* **298**, 284 (2001).
 52. O. Kraft, D. Saxa, M. Haag, and A. Wanner: The effect of temperature and strain rate on the hardness of Al and Al-based foams as measured by nanoindentation. *Z. Metallkde.* **92**, 1068 (2001).
 53. J. Xia, C.X. Li, and H. Dong: Hot-stage nano-characterizations of an iron aluminide. *Mater. Sci. Eng.* **A354**, 112 (2003).
 54. M. Hinz, A. Kleiner, S. Hild, O. Marti, U. Durig, B. Gotsmann, U. Drechsler, T.R. Albrecht, and P. Vettiger: Temperature dependent nano indentation of thin polymer films with the scanning force microscope. *Eur. Polym. J.* **40**, 957 (2004).
 55. T.G. Nieh, C. Iwamoto, Y. Ikuhara, K.W. Lee, and Y.W. Chung: Comparative studies of crystallization of a bulk Zr–Al–Ti–Cu–Ni amorphous alloy. *Intermetallics* **12**, 1183 (2004).
 56. X.G. Ma and K. Komvopoulos: In situ transmission electron microscopy and nanoindentation studies of phase transformation and pseudoelasticity of shape-memory titanium-nickel films. *J. Mater. Res.* **20**, 1808 (2005).
 57. Y.J. Zhang, Y.T. Cheng, and D.S. Grummon: Indentation stress dependence of the temperature range of microscopic superelastic behavior of nickel-titanium thin films. *J. Appl. Phys.* **033505**, 98 (2005).